Enhanced ferromagnetic transition temperature in NdO_xD_y epitaxial thin films

Dai Kutsuzawa,[1] Yasushi Hirose,[1] Yuki Sugisawa,[2] Junichi Kikuda,[2] Daiichiro Sekiba,[2,3] and Tetsuya Hasegawa[1]
[1]*Department of Chemistry, School of Science, The University of Tokyo, 7-3-1 Hongo, Bunkyo-ku, Tokyo 113-0033 Japan*
[2]*Graduate School of Pure and Applied Sciences, University of Tsukuba, Tennodai 1-1-1, Tsukuba, Ibaraki 305-8573, Japan*
[3]*Tandem Accelerator Complex, University of Tsukuba, 1-1-1 Tennoudai, Tsukuba, 305-8577 Japan*

(Received 20 November 2018; published 22 April 2019)

We investigated the electrical transport properties and magnetic properties of oxygen-containing fluorite-type neodymium dideuteride, NdO_xD_y, epitaxial thin films ($0.05 \leqslant x \leqslant 1.4$) grown on $CaF_2(111)$ substrate by a pulsed laser deposition technique. The NdO_xD_y thin films with $x \leqslant 0.3$ were crystallized in a pure fluorite phase, while the films with $x \geqslant 0.6$ were mixtures composed of fluorite and hexagonal Nd_2O_3-type phases. In the fluorite phase, ferromagnetism was observed from a magnetization loop and anomalous Hall effect. The films with $x < 1.4$ showed metallic transport properties with an abrupt drop of resistivity below Curie temperature T_C. With increasing x, T_C was raised to 10.0 K, which was higher than that of NdH_{2+x} with comparable carrier density.

DOI: 10.1103/PhysRevMaterials.3.044408

I. INTRODUCTION

Rare earth hydrides have wide tunability of their physical properties, such as optical, electrical transport, and magnetic properties, by adjusting the hydrogen content [1–5]. Recently, it has been reported that the properties can also be tuned by incorporation of oxygen. For example, the electrical resistivity of amorphous GdO_xH_y thin films is controllable in a wide range of 10^{-4}–$10^{10}\,\Omega\,\mathrm{cm}$ by changing the O/H ratio [6]. Oxygen-containing rare earth dihydrides, or rare earth oxyhydrides, LnO_xH_y (Ln = Y, Gd, Dy, and Er), show photochromism at ambient conditions [7–11], in contrast to pure hydrides exhibiting photochromism only under high pressure [12].

A remarkable feature of fluorite-type rare earth dihydrides is their magnetism. Most of them are antiferromagnetic at low temperature owing to Fermi surface topology [13,14], while NdH_2 shows ferromagnetism with Curie temperature T_C of 6.8 K [15], possibly due to large magnetoelastic coupling [14]. The T_C value was suppressed by insertion of excess hydrogen (NdH_{2+x}) at the octahedral site with concomitant decrease of carrier density [16,17]. Based on these observations, it has been argued that the magnetic interaction between Nd spins is mediated by conduction electron [Ruderman-Kittel-Kasuya-Yoshida (RKKY) interaction]. Oxygen incorporation is expected to modify the magnetic properties of NdH_2, because it would not only change the carrier density but also induce additional magnetic interaction between Nd ions through spatially more expended oxygen $2p$ orbital than hydrogen $1s$. However, there have not been many reports on magnetic properties of the rare earth oxyhydrides.

Here, we synthesized NdD_2 epitaxial thin films containing various amounts of oxygen, NdO_xD_y ($0.05 \leqslant x \leqslant 1.4$) and investigated their magnetic properties. The NdO_xD_y films with small oxygen contents ($x \leqslant 0.3$) were crystallized into a cubic fluorite phase, while oxygen-rich films ($x \geqslant 0.6$) were mixtures of fluorite and hexagonal Nd_2O_3-type structure phases. Magnetization and electrical resistivity measurements revealed enhanced T_C up to 10.0 K with increasing x.

II. EXPERIMENTAL PROCEDURE

NdO_xD_y thin films were grown on CaF_2 (111) substrate by using a reactive pulsed laser deposition technique. A Nd metal plate was ablated by a KrF excimer laser ($\lambda = 248$ nm) with a fluence of $0.77\,\mathrm{J\,cm^{-2}\,shot^{-1}}$ and a repetition rate of 5 Hz. The substrate temperature was maintained at 250 °C during the film growth. Prior to the film growth, the Nd target was thoroughly preablated in order to remove the surface oxide layer. Deuterium and oxygen gases were introduced into the chamber separately through two inlets, which were pointed to the substrate, to control the composition of the film (base pressure was below 9×10^{-7} Pa). Partial pressures of the process gases were carefully controlled by using variable leak valves. Under a relatively high-pressure condition ($P \geqslant 6.7 \times 10^{-1}$ Pa), a gate valve between the growth chamber and a molecular turbo pump [Shimadzu, TMP-803MC(0)] was partially closed to maintain the outlet pressure of the turbo molecular pump below 1.3×10^{-2} Pa. Note that heavy hydrogen (deuterium), not light hydrogen, was used to measure the hydrogen content in the film accurately, free from the contribution from surface adsorbed species such as water and hydrocarbon. The obtained NdO_xD_y films were covered with a several-nanometer-thick amorphous Si_3N_4 protection layer. The total film thickness was 50–150 nm, evaluated by a stylus profiler (Veeco, Dektak 6M).

The deuterium content y in the film was evaluated by elastic recoil detection analysis (ERDA) with a 2.5-MeV $^4He^{2+}$ beam (^{4}He-ERDA) conducted with a 1-MV electrostatic tandem accelerator at the Tandem Accelerator Complex, University of Tsukuba (UTTAC) [18]. The oxygen content x in the film was determined by energy dispersive x-ray spectroscopy in conjunction with a scanning electron microscope (SEM-EDX, JEOL, JSM-7100F with JED-

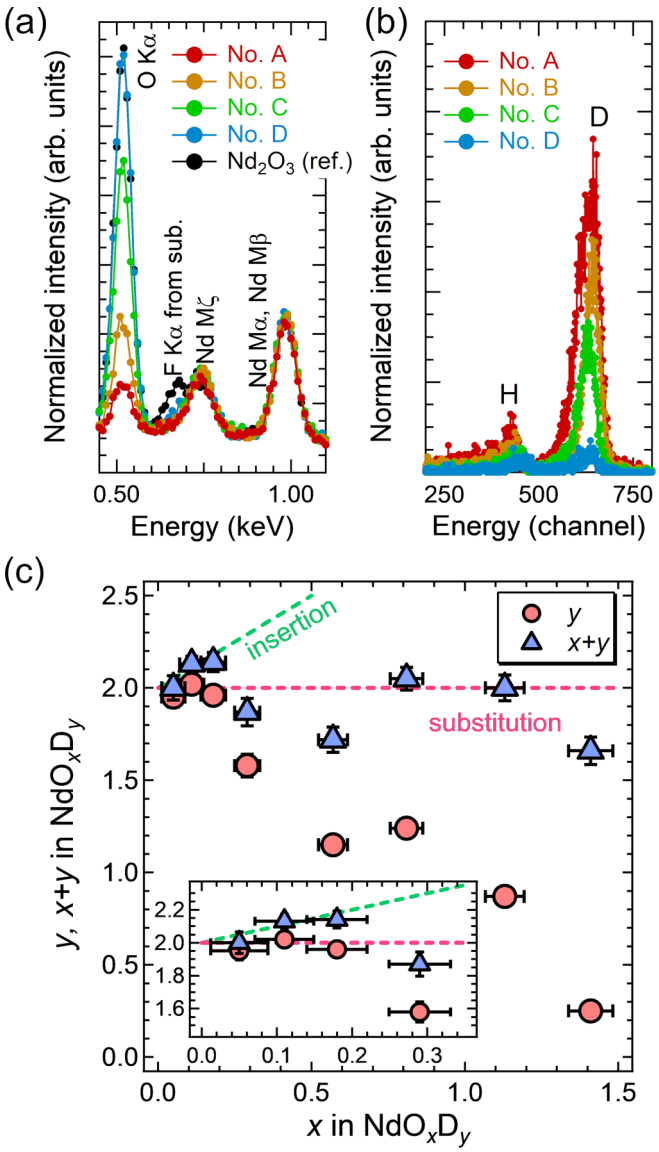

FIG. 1. (a) SEM-EDX and (b) ^{4}He-ERDA spectra of NdO_xD_y films. Note that the F $K\alpha$ peak derived from the substrate was observed in the EDX spectrum of the Nd_2O_3 film due to minimal thickness. (c) Deuterium content y and total anion content $x+y$ plotted against the oxygen content x. Inset in (c) is the enlarged figure in the region of $0 \leqslant x \leqslant 0.35$. Errors in x and y were within 0.07 and 0.06, respectively. Green and pink dashed lines are guides for $x+y$ in the case of hydrogen insertion and substitution, respectively.

2300), where the intensity was calibrated using a reference sample of which x was measured by a 38.4-MeV $^{35}Cl^{7+}$ beam (^{35}Cl-ERDA) using a 5-MV electrostatic tandem accelerator at the Micro Analysis Laboratory, Tandem accelerator (MALT), University of Tokyo (see Fig. 1 in the Supplemental Material [19]) [20]. Crystal structures of the films were determined by x-ray diffraction (XRD) with Cu $K\alpha_1$ radiation (Bruker AXS, D8 Discover), using one-dimensional array (VANTEC 1) and two-dimensional area (VANTEC 500) detectors. Electrical transport measurements were performed by the van der Pauw method with 100-nm-thick Ag electrodes using a physical property measurement system (Quantum Design, Model 6000). Magnetic properties were evaluated by a superconducting quantum interference device (SQUID) magnetometer (Quantum Design, MPMS-5S).

TABLE I. Process gas pressures during the film growth and anion composition of NdO_xD_y.

No.	P_{D2}(Pa)	P_{O2}(Pa)	x	y
A	6.7×10^{-1}		0.05 ± 0.04	2.0 ± 0.05
B	2.7×10^{-3}		0.3 ± 0.04	1.6 ± 0.06
C	2.7×10^{-3}	2.7×10^{-6}	0.8 ± 0.05	1.2 ± 0.03
D	2.7×10^{-3}	1.1×10^{-5}	1.4 ± 0.07	0.3 ± 0.02

III. RESULTS AND DISCUSSION

Figures 1(a) and 1(b) show SEM-EDX spectra and ^{4}He-ERDA spectra, respectively, of four typical NdO_xD_y films fabricated under various process gas conditions summarized in Table I. The EDX spectra were normalized by the Nd (Mα+Mβ) peak, and the oxygen content x was calculated by comparing the intensity ratio of the O $K\alpha$ peak and the Nd peak ($M\alpha + M\beta$) between the NdO_xD_y films and a Nd_2O_3 thin film as a reference. Note that a F $K\alpha$ peak originating from the CaF_2 substrate was observed in the EDX spectrum of the Nd_2O_3 film because the film was very thin. The ERDA spectra showed two peaks at energies (channel) of 430 and 640, which were assigned to hydrogen and deuterium, respectively, from comparison of their edge positions of the higher-energy side with those of a reference sample (amorphous carbon including both H and D) (Fig. 2 in the Supplemental Material [19]). The film fabricated under $P_{D2} = 6.7 \times 10^{-1}$ Pa without oxygen introduction (sample A) had a nearly stoichiometric composition of $x = 0.05$ and $y = 2.0$. By reducing P_{D2} to 2.7×10^{-3} Pa, x increased to 0.3 and y decreased to 1.6 (sample B). The oxygen in these films probably originated from residual gases, mainly water, in the fabrication chamber. Introduction of oxygen gas of $P_{O2} = 2.7 \times 10^{-6}$ Pa further increased x up to 0.8 with decrease of y down to 1.2 (sample C). Under higher $P_{O2} = 1.1 \times 10^{-5}$ Pa, x and y reached to 1.4 and 0.3, respectively (sample D). Figure 1(c) shows y and total anion content $x + y$ in various NdO_xD_y thin films as functions of x. There are two possible sites for oxygen to occupy in the fluorite lattice, the tetrahedral hydrogen site and the octahedral interstitial site. Although the local structure of the fluorite-type LnO_xH_y is still controversial, it was reported that both hydrogen and oxygen occupied the same tetrahedral site in stoichiometric oxyhydride, LnHO [21,22]. On the other hand, considering the ionic radii of H^- (127–152 pm) [23,24] and O^{2-} (142 pm) [25], insertion of oxygen at the octahedral site is also likely to occur. As seen in Fig. 1(c), when x was smaller than 0.3, y was almost constant at 2.0 within the measurement error range, and $x + y$ was monotonically increased with x, suggesting insertion of oxygen into an interstitial site. On the other hand, at $x \geqslant 0.3$, y tended to decrease with respect to x. This indicates that the introduced oxygen atoms were substituted for the deuterium sites.

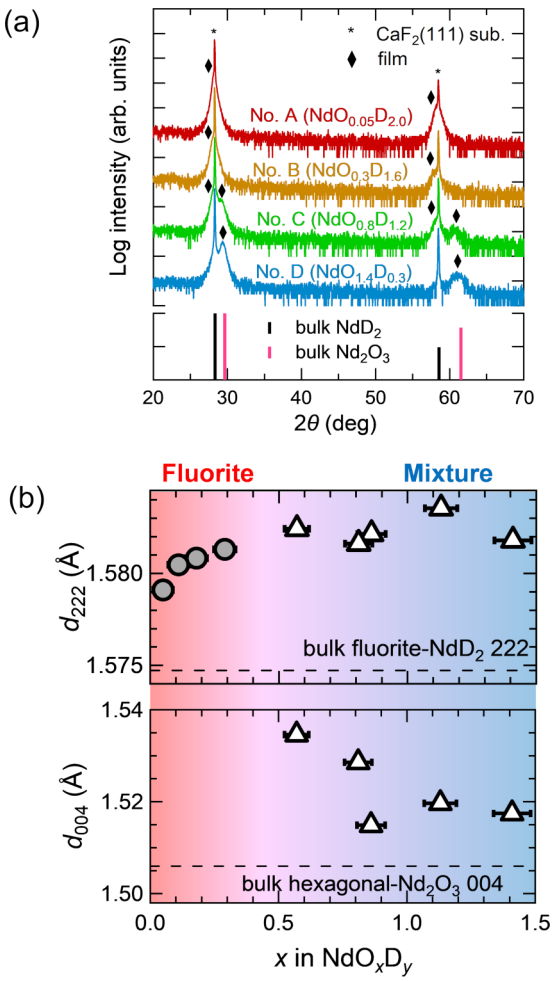

FIG. 2. (a) $2\theta/\theta$ XRD patterns of NdO_xD_y films grown on CaF_2 (111) substrate. Bar charts represent references of bulk NdD_2 *hhh* peaks [26] and bulk hexagonal-Nd_2O_3 00*l* peaks [27]. (b) *d* values of the NdO_xD_y films calculated from the fluorite 222 peak (top) and hexagonal 004 peak (bottom). The *d* value of $NdO_{1.4}D_{0.3}$ film was calculated from the −111 peak obtained by two-dimensional XRD (Fig. 3(d) in the Supplemental Material [19]) due to severe overlap of a substrate peak.

The oxygen content *x* was determined by EDX, where the EDX intensity was calibrated by a reference measured by ^{35}Cl-ERDA (Fig. 1 in the Supplemental Material [19]).

Figure 2(a) shows $\theta/2\theta$ XRD patterns of samples A–D. Sample A ($NdO_{0.05}D_{2.0}$) and B ($NdO_{0.3}D_{1.6}$) exhibited diffraction peaks on the left shoulders of the 222 and 444 peaks of the CaF_2 substrate. From two-dimensional detector images of asymmetric diffraction and φ scan plots (Figs. 3(a) and 3(b) in the Supplemental Material [19]), we determined that these films had the same fluorite structure as the CaF_2 substrate and undoped NdH_2 with twofold symmetric double domains. With further increase of *x*, unique diffraction peaks evolved at the right shoulders of the substrate peaks (sample C: $NdO_{0.8}D_{1.2}$), indicating the appearance of another phase. The intensity of these peaks increased with increasing *x*, and only these peaks were recognizable in the $\theta/2\theta$ XRD patterns of the most heavily oxygen-containing film (sample D: $NdO_{1.4}D_{0.3}$). The two-dimensional detector images

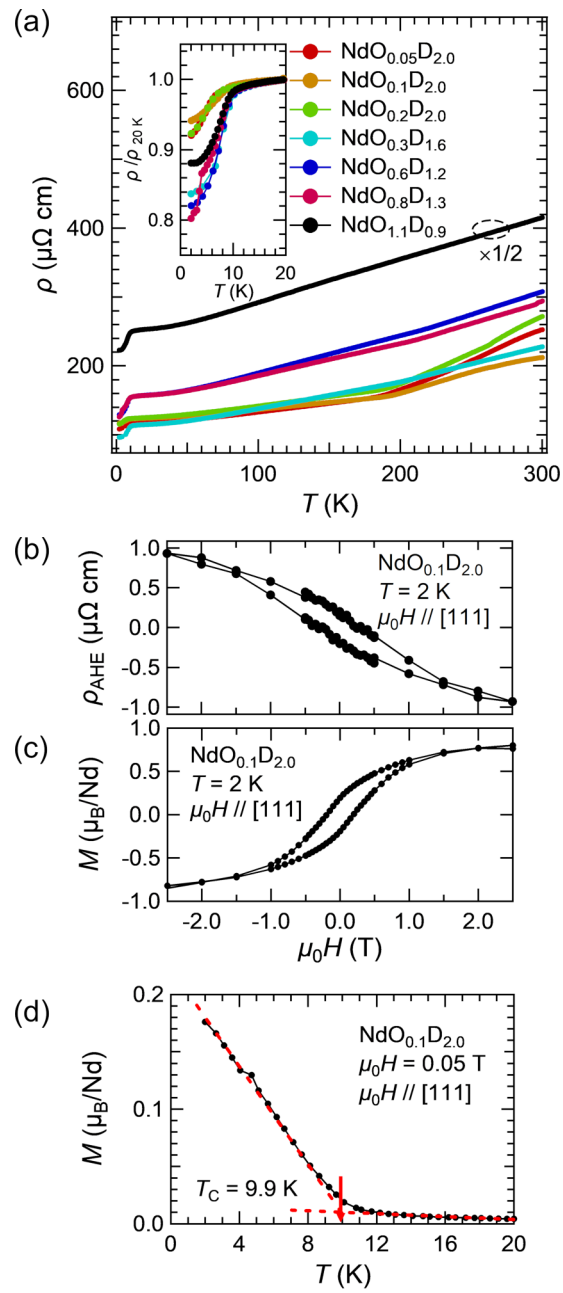

FIG. 3. (a) Temperature dependence of resistivity of the NdO_xD_y films. Inset shows the resistivity in the low-temperature region ($T \leqslant 20$ K) normalized by the resistivity at 20 K. (b) Anomalous Hall resistivity and (c) magnetization of the $NdO_{0.1}D_{2.0}$ film plotted against the magnetic field applied perpendicular to the film surface. (d) Temperature dependence of magnetization of the $NdO_{0.1}D_{2.0}$ film. Red dashed lines are the results of linear fitting in the vicinity of the magnetic transition temperature. T_C was determined as an intersection point of these lines.

of samples C and D revealed that these peaks originated from the hexagonal Nd_2O_3 structure (Fig. 3(c) in the Supplemental Material [19]). Note that even sample D contained a small amount of fluorite phase (supplemental Fig. 3(d) [19]). Figure 2(b) shows *x* dependence of *d* spacing calculated from the 222 peak of fluorite structure (d_{222}) and the 004 peak of hexagonal structure (d_{004}). In the small *x* region

($x \leqslant 0.3$), the NdO_xD_y film was a pure fluorite phase and d_{222} was expanded by increasing x. The d_{222} value of the fluorite structure became constant for the films with $x \geqslant 0.6$, indicating that the solubility limit of oxygen was around this value. Above the solubility limit, an oxygen-rich hexagonal phase appeared as the secondary phase. Hereafter we refer to the films with $x \leqslant 0.3$ and $x \geqslant 0.6$ as fluorite film and mixture film, respectively.

Next, we discuss the electrical transport properties and magnetic properties of the NdO_xD_y films. Figure 3(a) shows resistivity vs temperature (ρ-T) curves of the NdO_xD_y films with various anion compositions except for $NdO_{1.4}D_{0.3}$, of which resistivity was beyond the measurement limit. All of the ρ-T curves showed metallic behavior ($d\rho/dT > 0$) in the temperature range from 2 to 300 K. The fluorite films exhibited almost the same ρ for the entire temperature range, while ρ of the mixture films increased with increasing x. When plotting ρ at 300 K against the XRD peak area ratio of the fluorite 222 peak and hexagonal 004 peak (Fig. 4 in the Supplemental Material [19]), ρ and the ratio had a positive correlation. Thus, it is strongly suggested that the hexagonal phase is highly insulating and ρ is dominated by the electrical current passing through the conducting fluorite phase. The ρ-T curves of the oxygen-poor films ($NdO_{0.05}D_{2.0}$, $NdO_{0.1}D_{2.0}$, and $NdO_{0.2}D_{2.0}$) show a kink around 200 K, probably due to ordering of the deuterium sublattice, as observed in NdH_{2+x} with a variety of hydrogen contents [17]. The kink disappeared in the fluorite film with larger x ($x = 0.3$) and the mixture films ($x \geqslant 0.6$), implying that oxygen incorporated into the deuterium site of fluorite NdD_2 suppressed the ordering of the deuterium sublattice. The inset of Fig. 3(a) shows ρ-T curves at the low-temperature region ($T \leqslant 20$ K), where ρ was normalized by the value at 20 K. All of the films showed an abrupt drop of ρ around 10 K or lower. Below this temperature, we observed the anomalous Hall effect with a hysteresis loop [Fig. 3(b)], of which the curve shape resembled the magnetization vs magnetic field loop [Fig. 3(c)]. Therefore, we concluded that the NdO_xD_y films underwent ferromagnetic transition at this temperature. The reduction of ρ below T_C can be attributed to suppression of electron scattering by randomly oriented spins, as reported in NdH_{2+x} [15].

To discuss the influence of oxygen incorporation on the magnetic phase transition, we evaluated T_C from the ρ-T curves as an intersection of two linear lines obtained by fitting in the slightly higher- and lower-temperature regions (Fig. 5 in the Supplemental Material [19]). The T_C value deduced from the fluorite-$NdO_{0.1}D_{2.0}$ film was 9.6 K, which agreed well with that determined from the magnetization vs temperature curve [$T_C = 9.9$ K, Fig. 3(d)]. Figure 4(a) plots T_C of the NdO_xD_y films against x. The least-oxygen-containing film ($NdO_{0.05}D_{2.0}$) showed T_C of 7.4 K, which was comparable to the reported values for stoichiometric NdH_2 (5.6 K [28]) and 6.8 K [15]). With increasing x, T_C increased and reached 10.0 K in $NdO_{0.3}D_{1.6}$, in sharp contrast to NdH_{2+x}, in which T_C is lowered by introduction of excess hydrogen. No further increase of T_C was observed in the mixture films ($x \geqslant 0.6$).

The ferromagnetic ordering in NdH_2 is understood in terms of RKKY interaction [15,28], and in this scenario, the decrease of T_C with the introduction of excess hydrogen

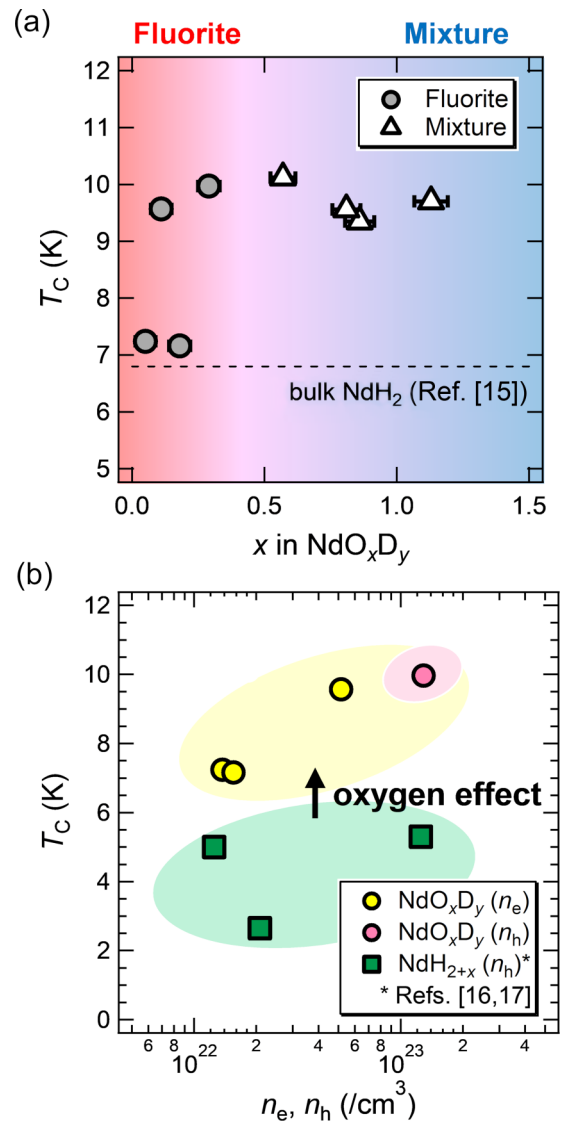

FIG. 4. (a) Oxygen content x dependence of T_C of the NdO_xD_y films. Filled circle and open triangle symbols denote T_C of the fluorite and the mixture films, respectively. Dashed line refers to T_C of bulk NdH_2 [15]. (b) T_C plotted against carrier density (n_e or n_h) of the fluorite NdO_xD_y films evaluated by Hall measurements at 2 K, where n_e and n_h stand for the densities of electron and hole carriers, respectively. The figure also includes the n_h values of NdH_{2+x} measured at 473 K [16,17]. The oxygen-inserted NdO_xD_y film ($x \leqslant 0.2$, yellow filled circle) showed n-type conduction, while the oxygen-substituted NdO_xD_y film ($x = 0.3$, red filled circle) and NdH_{2+x} (green filled square) showed p-type conduction.

can be explained by decrease of carrier density [16,17]. The carrier density of the fluorite NdO_xD_y films evaluated from Hall resistivity in the high-magnetic-field region was shown in Fig. 4(b) (see also Fig. 6 in the Supplemental Material [19]). Interestingly, the carrier density, or Hall coefficient of NdO_xD_y behaved very differently from those of NdH_{2+x} and other rare earth dihydrides (supplemental Fig. 7 [19]). Notably, the fluorite NdO_xD_y films with inserted octahedral oxygen ($x \leqslant 0.2$) exhibited n-type conduction in contrast to NdH_{2+x}, which is known to behave as a p-type conductor

[16]. We speculate that the n-type conduction in lightly oxygen-containing fluorite NdO_xD_y films was due to formation of a deep impurity band mainly composed of an oxygen $2p$ orbital hybridized with a Nd $5d$ orbital, which reduces the number of electrons in the Nd $5d$ orbital-nature conduction band. Further oxygen introduction first increased the carrier density but finally caused carrier-type inversion from n type to p type at $x = 0.3$, although the mechanism of the carrier-type inversion is not clear at present. Despite the change in carrier type between $x = 0.2$ and 0.3, T_C of the fluorite NdO_xD_y films was positively correlated with carrier density, as shown in Fig. 4(b), supporting the RKKY scenario. However, T_C of NdO_xD_y was much higher than that of NdH_{2+x} with comparable carrier densities [16,17], implying that there is yet another factor having a large influence on T_C, such as magnetic interaction through the extended orbital of oxygen.

IV. CONCLUSION

We systematically examined the effect of oxygen incorporation on the electrical transport and magnetic properties of NdD_2 epitaxial thin films. In the lightly oxygen-containing films ($x \leqslant 0.3$), oxygen was introduced into the NdD_2 lattice while maintaining the fluorite structure. Anion composition analysis suggested oxygen insertion at the octahedral site ($x \leqslant 0.2$), followed by oxygen substitution for the tetrahedral hydrogen site ($x = 0.3$) in the fluorite NdD_2. In contrast, when the oxygen content was larger ($x \geqslant 0.6$), an oxygen-rich hexagonal Nd_2O_3-type structure appeared as the secondary phase. By increasing x, T_C of the fluorite NdO_xD_y was enhanced from 7.4 K ($NdO_{0.05}D_{2.0}$) to 10.0 K ($NdO_{0.3}D_{1.6}$), accompanied with carrier-type inversion from n type to p type. The maximum T_C value of NdO_xD_y was considerably higher than that of NdH_{2+x} with comparable carrier density. This result suggested that the O $2p$ orbital having more extended character than H $1s$ enhanced the magnetic interaction between Nd ions through Nd-O hybridization.

ACKNOWLEDGMENTS

We thank Prof. Hiroyuki Matsuzaki of the University of Tokyo for his assistance with the ^{35}Cl-ERDA measurements and Mr. Satoshi Ishii of University of Tsukuba for his assistance with the ^{4}He-ERDA measurements. Magnetic property measurements were performed using facilities of the Cryogenic Research Center, the University of Tokyo. This study was supported by the Grant-in-Aid for Scientific Research in the Innovation Area "Mixed anion" (Grants No. JP16H06438 and No. JP16H06441) from the Japan Society for the Promotion of Science (JSPS). One of the authors (D.K.) was also supported by the JSPS through the Program for Leading Graduate Schools (MERIT).

[1] J. N. Huiberts, R. Griessen, J. H. Rector, R. J. Wijngaarden, J. P. Dekker, D. G. de Groot, and N. J. Koeman, Nature **380**, 231 (1996).
[2] P. Vajda, in *Handbook on the Physics and Chemistry of Rare Earths*, Vol. 20, edited by K. A. Gschneider, Jr. and L. Eyring (Elsevier, Amsterdam, 1995), pp. 207–291.
[3] P. Vajda, Phys. B (Amsterdam, Neth.) **289–290**, 435 (2000).
[4] P. H. L. Notten, Curr. Opin. Solid State Mater. Sci. **4**, 5 (1999).
[5] P. Vajda, J. Alloys Compd. **231**, 170 (1995).
[6] A. Miniotas, B. Hjörvarsson, L. Douysset, and P. Nostell, Appl. Phys. Lett. **76**, 2056 (2000).
[7] T. Mongstad, C. Platzer-Björkman, J. P. Maehlen, L. P. A. Mooij, Y. Pivak, B. Dam, E. S. Marstein, B. C. Hauback, and S. Z. Karazhanov, Sol. Energy Mater. Sol. Cells **95**, 3596 (2011).
[8] F. Nafezarefi, H. Schreuders, B. Dam, and S. Cornelius, Appl. Phys. Lett. **111**, 103903 (2017).
[9] J. Montero, F. A. Martinsen, M. Lelis, S. Z. Karazhanov, B. C. Hauback, and E. S. Marstein, Sol. Energy Mater. Sol. Cells **177**, 106 (2018).
[10] C. C. You, D. Moldarev, T. Mongstad, D. Primetzhofer, M. Wolff, E. S. Marstein, and S. Z. Karazhanov, Sol. Energy Mater. Sol. Cells **166**, 185 (2017).
[11] J. Montero, F. A. Martinsen, M. García-Tecedor, S. Z. Karazhanov, D. Maestre, B. Hauback, and E. S. Marstein, Phys. Rev. B **95**, 201301(R) (2017).
[12] A. Ohmura, A. MacHida, T. Watanuki, K. Aoki, S. Nakano, and K. Takemura, Appl. Phys. Lett. **91**, 151904 (2007).
[13] G. Wiesinger and G. Hilscher, Handb. Magn. Mater. **6**, 511 (1991).
[14] S. H. Liu, Solid State Commun. **61**, 89 (1987).
[15] S. Senoussi, J. N. Daou, P. Vajda, and J. P. Burger, J. Less-Common Met. **130**, 55 (1987).
[16] R. C. Heckman, J. Chem. Phys. **48**, 5281 (1968).
[17] J. N. Daou, J. P. Burger, and P. Vajda, Philos. Mag. B **65**, 127 (1992).
[18] D. Sekiba, N. Takemoto, M. Okada, S. Ishii, T. Sakurai, and K. Akimoto, Diamond Relat. Mater. **27–28**, 60 (2012).
[19] See Supplemental Material at http://link.aps.org/supplemental/10.1103/PhysRevMaterials.3.044408 for oxygen content x in the NdO_xD_y films measured by SEM-EDX and ^{35}Cl-ERDA, ^{4}He-ERDA spectra of an amorphous carbon film including H and D, 2D-XRD pattern of Sample No. A ($NdO_{0.05}D_{2.0}$), φ scan of fluorite-type $NdO_xD_y\{200\}$ peak, 2D-XRD patterns around the CaF_2 202 and CaF_2 200 diffractions of sample D ($NdO_{1.4}D_{0.3}$), resistivity of the mixture NdO_xD_y films at 300 K plotted against the XRD intensity ratio between fluorite-type phase 222 peak and hexagonal-type phase 004 peak, temperature-dependent resistivity of $NdO_{0.1}D_{2.0}$ film, Hall resistivity ρ_{xy} of the fluorite NdO_xD_y films as a function of magnetic flux density $\mu_0 H$, and Hall coefficient of the fluorite NdO_xD_y films and rare earth dihydrides evaluated by Hall measurements.
[20] I. Harayama, K. Nagashima, Y. Hirose, H. Matsuzaki, and D. Sekiba, Nucl. Instrum. Methods Phys. Res., Sect. B **384**, 61 (2016).
[21] J. Ueda, S. Matsuishi, T. Tokunaga, and S. Tanabe, J. Mater. Chem. C **6**, 7541 (2018).
[22] H. Yamashita, T. Broux, Y. Kobayashi, F. Takeiri, H. Ubukata, T. Zhu, M. A. Hayward, K. Fujii, M. Yashima, K. Shitara, A.

Kuwabara, T. Murakami, and H. Kageyama, J. Am. Chem. Soc. **140**, 11170 (2018).

[23] R. D. Shannon, Acta Crystallogr., Sect. A **32**, 751 (1976).

[24] H. Kageyama, K. Hayashi, K. Maeda, J. P. Attfield, Z. Hiroi, J. M. Rondinelli, and K. R. Poeppelmeier, Nat. Commun. **9**, 772 (2018).

[25] R. D. Shannon and C. T. Prewitt, Acta Crystallogr., Sect. B: Struct. Crystallogr. Cryst. Chem. **25**, 925 (1969).

[26] H. Müller, P. Knappe, and O. Greis, Z. Phys. Chem. **114**, 45 (1979).

[27] W. Zachariasen, Z. Phys. Chem. **119U**, 201 (1926).

[28] R. L. Carlin, L. J. Krause, A. Lambrecht, and H. Claus, J. Appl. Phys. **53**, 2634 (1982).